Combustion and Flame 270 (2024) 113728

Contents lists available at ScienceDirect

Combustion and Flame

journal homepage: www.sciencedirect.com/journal/combustion-and-flame

Theoretical studies of supercritical real-fluid oxidations of diverse fuels by using the 3rd-order virial equation of state with nonlinear effects

Junfeng Bai [a,b], Xin Zhang [a], Chong-Wen Zhou [c], Peng Zhang [b], Hao Zhao [a,*]

[a] College of Engineering, Peking University, Beijing 100871, PR China
[b] Department of Mechanical Engineering, City University of Hong Kong, Kowloon Tong, Kowloon, 999077, Hong Kong
[c] School of Energy and Power Engineering, Beihang University, Beijing 100191, PR China

ARTICLE INFO

Keywords:
Real fluid
Thermodynamics
Virial equation of state
Supercritical modelling
Diverse fuels

ABSTRACT

The 3rd-order Virial equation of state (EoS) with nonlinear effects was constructed and applied to simulate various real-fluid fuel oxidations, including hydrocarbons and oxygenated fuels under supercritical conditions. The real-fluid effects for hydrocarbon and oxygenated fuel oxidations have been discussed by using the Redlich-Kwong (RK) and the 3rd-order Virial methods. The compressibility factors calculated using the 3rd-order Virial EoS possess better agreements with experimental data for H_2, N_2, and H_2O at different temperatures and below 300 atm than the previous 2nd-order Virial EoS and the RK EoS. The calculations of thermodynamic properties by using the 3rd-order Virial EoS also showed a better agreement with experimental data for H_2O than using the RK EoS. The RK method exhibited contradictory speciation predictions against the ideal-gas 0-D and 1-D simulations in H_2O and N_2/CO_2 diluent gases, respectively, while the 3rd-order Virial method kept its consistency. Especially, the ignition delay simulation by using the 3rd Virial EoS is extended to the operation conditions relevant to the recent SpaceX Starship Raptor engines in CH_4/O_2 mixture at 600 atm. It shows the decreases in the ignition delay times by 3 times by including the real-fluid impact. The simulation results were also compared with a series of existing experimental data for ammonia, larger alkanes, and gasoline blends, which show significant real-fluid effects at low temperatures. Instead of inputting critical pressure and temperature parameters of different species manually in the typical empirical methods with high inconvenience and uncertainties, the required parameters in the 3rd-order Virial method can be directly obtained from the input transport document for real-fluid computations.

Novelty and significance statement

The novelty of this combustion simulation study is the development of the 3rd-order Virial equation of state (EoS) the application to simulate various real-fluid fuel oxidations, including hydrocarbons and oxygenated fuels under supercritical conditions. The real-fluid effects of EoS, thermodynamics, and chemical potential have been investigated on the freely propagating flame simulations of different fuels, respectively. The 3rd-order Virial method provides better estimations of the real-fluid behaviors than the empirical RK method, especially at high pressures.

1. Introduction

Supercritical combustion in advanced engines and gas turbines has been drawing more attention recently due to high thermodynamic efficiency and low emissions [1-6]. It has already been directly applied in rocket engines and high-pressure diesel engines. For example, the raptor engines in the recent SpaceX Starship [7] are operated under pressures above 300 atm by using CH_4/O_2 mixture in supercritical combustion conditions. Its launch misfire and failure are highly relevant to supercritical CH_4 combustion and flame instabilities. Therefore, understanding the supercritical reaction kinetics is crucial for designing the above energy conversion systems and optimizing their burning strategies [1,3]. However, the real-fluid effects on combustion modeling need to be carefully considered due to the failure of ideal-gas assumptions at such high pressures, and real-fluid molecular volume and interaction

* Corresponding author.
E-mail address: h.zhao@pku.edu.cn (H. Zhao).

https://doi.org/10.1016/j.combustflame.2024.113728
Received 1 May 2024; Received in revised form 9 September 2024; Accepted 10 September 2024
Available online 13 September 2024

potential cannot be ignored [8]. Accurate descriptions of real-fluid effects on the equation of state (EoS), thermodynamics properties, chemical potentials, and overall reactive flow simulations are crucial for investigating supercritical combustion [9].

A series of empirical real-fluid EoSs were proposed in the last century, including Van de Waals EoS [10], Redlich-Kwong (RK) EoS [11,12], Soave-Redlich-Kwong (SRK) EoS [13], and Peng-Robinson (PR) EoS [14], and they were incorporated into combustion model simulations very recently [4,9,15]. Kogekar et al. [9] studied the non-ideal effects on the ignition delay times of n-dodecane in high-pressure shock tubes by using RK EoS in the Cantera program. Liang et al. [4] studied real-fluid thermodynamics and transport properties based on SRK EoS by using the CHEMKIN code. The effects of thermodynamics and transport properties were discussed respectively on hydrogen/air and methane/air flame speed predictions at supercritical conditions. Li et al. [15] simulated hydrogen oxidation in supercritical water/carbon dioxide mixtures by using PR EoS. However, the empirical methods in the literature lack physical insights into molecular interactions and molecular polarizations and may result in significant generalization uncertainties beyond training datasets. Moreover, in the empirical methods, critical pressures and temperatures of molecules and radicals are needed to provide either from literature or by computational estimations as additional input information in the Cantera and CHEMKIN software, resulting in high inconvenience and uncertainties in the real-fluid combustion simulations of large molecules.

Liang et al. [4] evaluated critical pressures and temperatures of radicals by l-J potential parameters [16] in the methane system. Kogekar et al. [9] estimated these critical properties involved in the n-dodecane mechanism by using the Joback group contribution method [17,18]. Due to the lack of consistent methods in estimating critical pressures and temperatures of molecules and radicals, the simulation results of different fuels and summarized rules of real-fluid effects in literature lack consistency and universality, and they are hard to be repeated and validated.

The Virial EoS was used to describe real-fluid behaviors on hydrogen oxidation in previous work [19-23]. Different from the empirical EoS methods (e.g. RK, SRK, PR methods) used in literature, the Virial method contains deeper-level physical insights, including real-fluid partition function calculations, intermolecular potentials, and molecular polarizations. Moreover, empirical EoSs are fitted by using critical pressures and temperatures as fixed points. This treatment may cause significant deviations at conditions far away from critical points. For example, the Virial method reveals better performance in computing the thermodynamic property calculations of water than the RK method [22].

In this work, the 3rd-order Virial method with nonlinear effects, including the corrections of real-fluid EoS, thermodynamics properties, and chemical potentials, was developed and incorporated into the Cantera program for the reactive real-fluid simulations of various hydrocarbon and oxygenated fuels. Instead of inputting critical pressure and temperature parameters of molecules and radicals manually from literature or computational estimations in the typical empirical methods, the required parameters for different species in the 3rd-order Virial method can be directly and conveniently obtained from the input transport document. It enables to simulate supercritical oxidation of different fuels with known transport parameters easily. The real-fluid effects on compressibility factors, thermodynamic properties, and chemical potentials for methane oxidation in supercritical water have been discussed respectively. Comparisons between the real-fluid simulations of ammonia and larger fuels and experimental data in literature have also been provided. This work provides a consistent and universal method for computing high-pressure real-fluid properties and predicting reactive real-fluid behaviors with high accuracies. The 3rd-order Virial method in this work is incorporated in the open-source Cantera program for real-fluid computations.

2. Theoretical methods

The Virial EoS [21] is used to describe real-fluid behaviors.

$$\frac{p\widetilde{V}}{RT} = 1 + \frac{B(T)}{\widetilde{V}} + \frac{C(T)}{\widetilde{V}^2} + O\left(\widetilde{V}^{-3}\right) \tag{1}$$

where the temperature-dependent coefficient $B(T)$ and $C(T)$ are called the second and third Virial coefficients; $B(T)/\widetilde{V}$ presents the linear effects, $C(T)/\widetilde{V}^2$ presents the nonlinear effects, $O\left(\widetilde{V}^{-3}\right)$ presents the infinitesimal of higher order; p, $\widetilde{V}$, T are pressure, molar volume, and temperature; R is the ideal gas constant; the terms on the RHS of Eq. (1) represents the correction of real-fluid effects in the decreasing order of $\widetilde{V}$ [20]. The expressions of 3rd-order Virial coefficients can be derived from real-fluid partition function calculations based on different intermolecular potential models under the Boltzmann distribution [21].

Based on the 3rd-order Virial EoS, Lennard-Jones (L-J) (6–12) potential [24] and Stockmayer potential [19,25], the corrections of real-fluid thermodynamics and chemical potentials [9] are also derived and extended from hydrogen to various fuels in this work by using the transport properties of different species.

The real-fluid corrections of thermodynamics properties from ideal values ($\widetilde{H}-\widetilde{H}^0$, $\widetilde{S}-\widetilde{S}^0$, $\widetilde{C}_p-\widetilde{C}_p^0$) can be computed by:

$$\frac{\widetilde{H}-\widetilde{H}^0}{R} = T^\star\left\{\frac{B^\star - B_1^\star}{V^\star} + \frac{C^\star - \frac{1}{2}C_1^\star}{(V^\star)^2}\right\} \tag{2}$$

$$\frac{\widetilde{S}-\widetilde{S}^0}{R} = -\left\{\frac{B_1^\star}{V^\star} + \frac{(B^\star)^2 - C^\star + C_1^\star}{2(V^\star)^2}\right\} \tag{3}$$

$$\frac{\widetilde{C}_p-\widetilde{C}_p^0}{R} = -\frac{B_2^\star}{V^\star} + \frac{\left(B^\star - B_1^\star\right)^2 - C^\star + C_1^\star - \frac{1}{2}C_2^\star}{(V^\star)^2} \tag{4}$$

where $B^\star$, $B_1^\star$, $B_2^\star$, $C^\star$, $C_1^\star$ and $C_2^\star$ are dimensionless Virial coefficient and its first- and second-order derivative, $T^\star$ and $V^\star$ are dimensionless temperature and volume.

All derived equations applied to the various reaction simulations have been incorporated into the Cantera Code [26] and packed as the real-fluid 3rd-order Virial model to implement the real-fluid simulations in this work.

The RK EoS is:

$$p = \frac{RT}{\widetilde{V}-b} - \frac{a}{\widetilde{V}\sqrt{T}(\widetilde{V}+b)} \tag{5}$$

where a and b are parameters describing real-fluid effects, and they are computed using critical properties. The advantages of the 3rd-order Virial method are obvious compared to the RK method. The 3rd-order Virial method contains deeper-level physical insights by including real-fluid partition function, intermolecular potentials, and molecular polarizations. Additionally, for a detailed mechanism of larger fuels with more species involved, the determination of parameters describing real-fluid behaviors in RK EoS is complicated. Liang et al. [4] evaluated parameters a and b of species by critical properties, while critical properties of radicals were estimated by l-J potential parameters [16] in the methane system. Kogekar et al. [9] estimated the critical properties of radical species involved in the n-dodecane mechanism by using the Joback method [17,18]. Namely, a user needs to process numerous complicated parameter estimations for every input mechanism by using empirical methods, which increases significant workload and unavoidable uncertainties in different parameter evaluation methods. Moreover, the simulation results lack consistency and universality due to different treatments for parameter estimations in the literature. However, for the

3rd-order Virial method, the estimation of l-J potential parameters is not necessary as they are already provided for different molecules and radicals in transport input files. Therefore, the required l-J potential parameters in the 3rd-order Virial method can be directly acquired from the transport input document by using a simple script file. The real-fluid behaviors can be discussed respectively for diverse fuels based on consistent l-J potential parameters, avoiding extra uncertainties in parameter estimations for a real-fluid equation of state. This is another obvious advantage of the 3rd-order Virial method rather than the RK method.

The difference of the computation method used in this work compared to our previous work [22] is shown in Table 1. 1) The 3rd-order Virial method with nonlinear effects, including the corrections of real-fluid EoS, thermodynamics properties, and chemical potentials, was developed and incorporated into the Cantera program in the present work. It improves the predictions of compressibility factors, compared to the previous 2nd-order method. 2) The range of application extends from hydrogen to various hydrocarbon and oxygenated fuels in the present work. 3) The required parameters for different species in the 3rd-order Virial method can be directly and conveniently obtained from the input transport document, instead of inputting critical pressure and temperature parameters of molecules and radicals manually from literature or computational estimations in the typical empirical methods.

3. Results and discussion

3.1. The 3rd-order virial EoS

In our previous work [22], the calculations of compressibility factors by employing the 2nd-order Virial EoS show better consistency with JANAF experimental data [27] below 200 atm than the RK method, especially for dilute gases N_2, CO_2, and H_2O. However, its predictions become worse above 200 atm.

Therefore, the 3rd-order Virial EoS was constructed and applied to simulate various real-fluid fuel oxidations, including hydrocarbons and oxygenated fuels under supercritical conditions in this work. The compressibility factors computed by employing the 3rd-order Virial EoS and the RK EoS are shown in Fig. 1. It shows that the compressibility factors calculated using the 3rd-order Virial EoS possess better agreements with experimental data for H_2, N_2, and H_2O at different temperatures below 300 atm, especially for the predictions of H_2O. According to Fig. 2, the compressibility factors computed by employing the 3rd-order Virial EoS show more improvements than the previous 2nd-order Virial EoS referring to experimental data of pure N_2, H_2, and H_2O.

3.2. Comparison for thermodynamic properties corrections

Corrections of thermodynamic properties, such as enthalpy (H), heat capacity (C_p), and entropy (S), for pure H_2O at 100 atm are calculated using the 2nd and 3rd-order Virial EoS and the RK EoS and are compared with the JANAF data [27], which is from direct measurement or extrapolation, in Fig. 3. It shows that the real-fluid corrections of enthalpy and heat capacity using both the 2nd and 3rd-order Virial EoS show improved agreements with the JANAF data than using the RK EoS. The difference between the entropy corrections using the 2nd and 3rd-order Virial EoS and in the JANAF table is insignificant. Due to underestimation of real-fluid effects on heat capacity using the RK EoS, deeper weakness may appear in its adiabatic simulations. In addition, the predicted real-fluid heat capacity is about 20 % larger than the ideal-gas value of H_2O ($C_p = 38.7$ J/mol K^{-1} at 800 K [34]) at 800 K and 100 atm, resulting in a potential 20 % deviation of temperature in ideal-gas adiabatic simulations.

Table 1
The differences of the methods and simulations used in this work compared to our previous work.

Differences	The previous work	This work
The Virial method	2nd-order	3rd-order with nonlinear effects
Range of application	Hydrogen	various hydrocarbon and oxygenated fuels
Real-fluid parameters	manually inputted	obtained from the input transport document

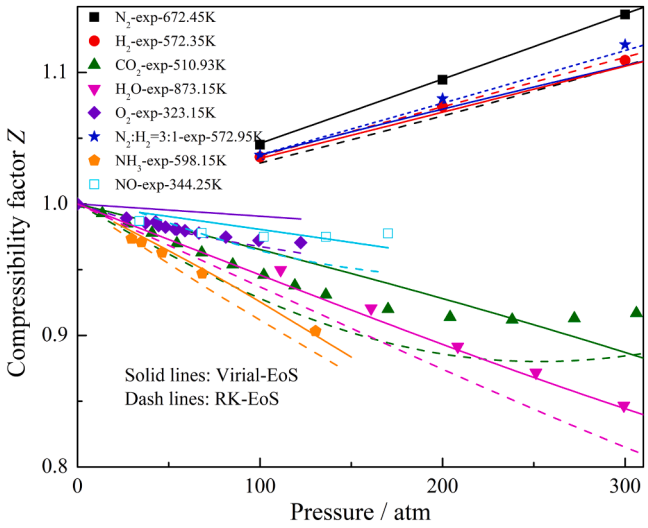

Fig. 1. The compressibility factors computed by employing the 3rd-order Virial EoS and the RK EoS with comparison to experimental data of pure N_2 [28], H_2 [28], CO_2 [29], H_2O [30], O_2 [31], NH_3 [32], NO [33] and mixture of N_2 and H_2 [28].

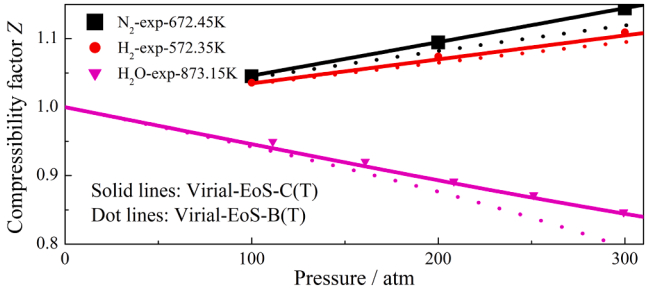

Fig. 2. The compressibility factors computed by employing the 3rd-order Virial EoS and the 2nd-order Virial EoS with comparison to experimental data of pure N_2 [28], H_2 [28], and H_2O [30].

3.3. The simulations for methane

The real-fluid impact of compressibility factors, real-fluid thermodynamics properties, and real-fluid chemical potentials on the simulations of hydrocarbon oxidation have been studied in this work. The oxidation of methane is taken as an example to investigate real-fluid effects on the simulations.

The 3rd-order Virial method and the RK method were modified to consider (a): real-fluid EoS only; (b): real-fluid thermodynamic properties only; (c): real-fluid chemical potentials only; (d): total effects. The methane oxidation are performed in a 0-D, adiabatic, homogenous reactor using H_2O as diluent gas at 300 atm, and are shown in Fig. 4. In Fig. 4(a), only the effects of compressibility factors were considered. The formulas of volume computations were changed based on 3rd-order Virial EoS and RK EoS while ideal-gas thermodynamics properties and chemical potentials were used. The oxidations increase using both real-fluid methods because of the increase of density in real-fluid than the ideal-gas case.

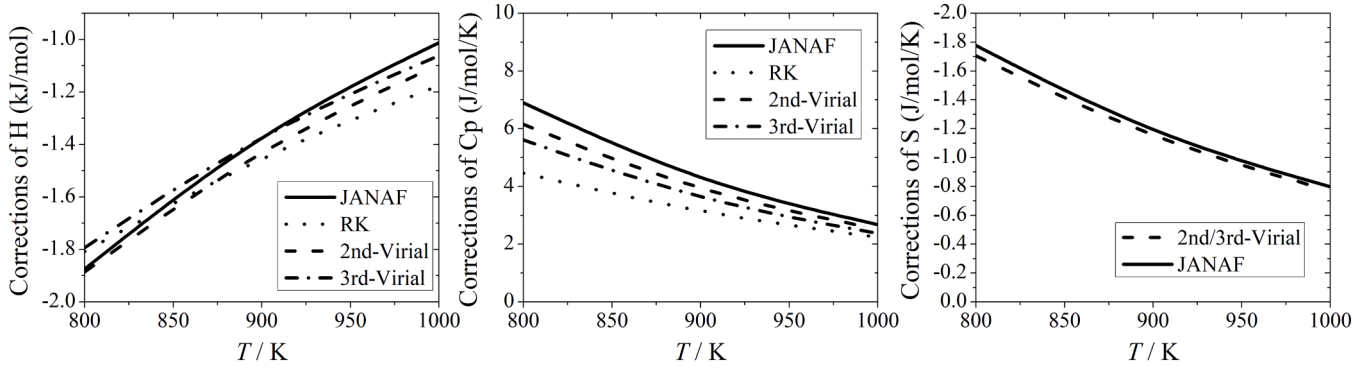

Fig. 3. Real-fluid corrections of thermodynamic properties enthalpy (H), heat capacity (Cp), and entropy (S) for pure H_2O at 100 atm calculated using the 2nd/3rd-order Virial EoS and the RK EoS and comparison with JANAF data.

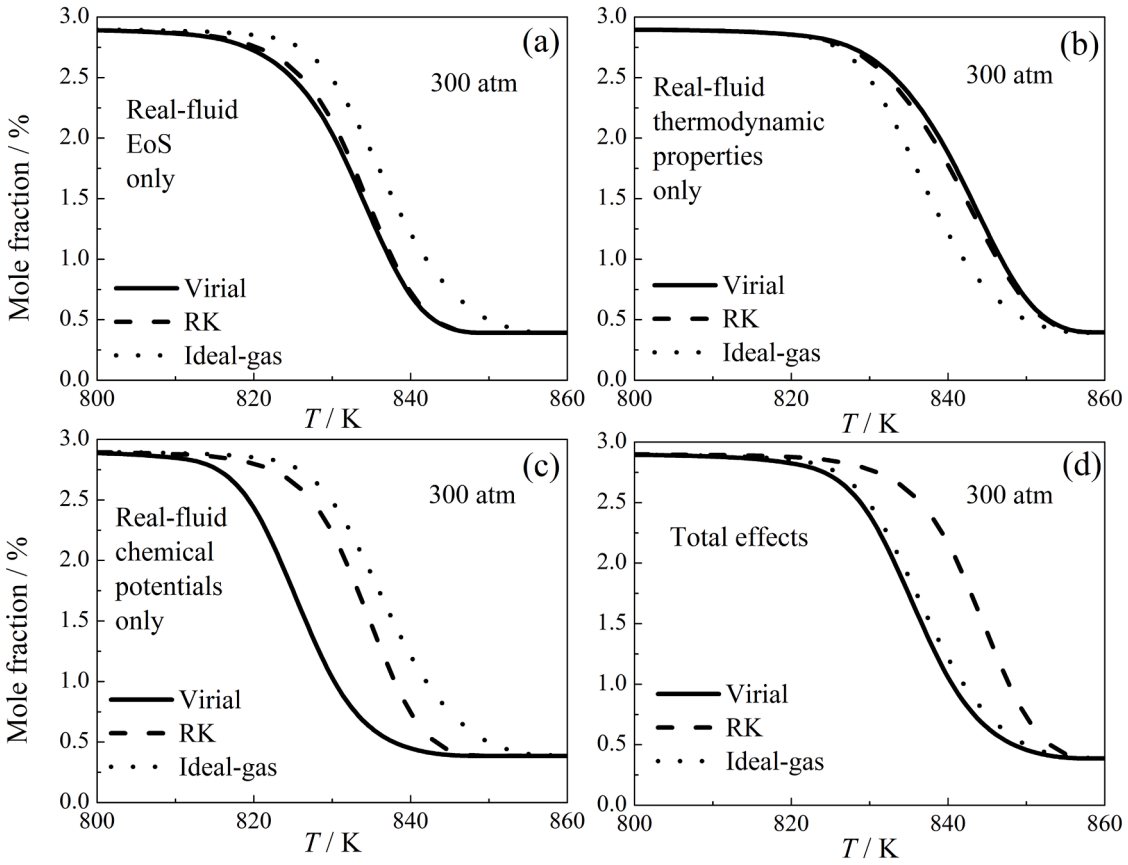

Fig. 4. The speciation simulations of methane in a 0-D adiabatic, homogenous reactor using H_2O as diluent gas at 300 atm by using the 3rd-order Virial, RK, and ideal-gas methods. (a): real-fluid EoS only; (b): real-fluid thermodynamic properties only; (c): real-fluid chemical potentials only; (d): total effects. CH_4:O_2:H_2O = 2.9:4.24:92.86. Residence time = 295 K * 0.15 s / T.

In Fig. 4(b), only the effects of real-fluid thermodynamics properties were considered. The corrections of real-fluid thermodynamics properties in the 3rd-order Virial and the RK methods were used, while ideal-gas EoS and chemical potentials formulas were fixed. The major impact of real-fluid thermodynamics properties comes from the increase of heat capacity, especially in H_2O diluent gas. The increase in heat capacity will result in a decrease in system temperature in the adiabatic simulation, to inhibit the methane oxidation. Namely, the reactivities decrease with the effects of real-fluid thermodynamics properties. The corrections of thermodynamics properties of pure H_2O computed by using the Virial method [22] are more accurate than using the RK method referring to the JANAF table [27]. Since the heat capacity computed by using the Virial method is larger than that using the RK method, the inhibiting effect is more distinct by using the Virial method than the RK method.

In Fig. 4(c), only the effects of real-fluid chemical potentials were considered. Real-fluid chemical potential corrections were employed while ideal-gas EoS and thermodynamics properties were kept. With molecular interactions in real-fluid methods, the collision and consumption rates of fuel mixtures tend to be accelerated. Hence, the reactivities increase with the impact of real-fluid chemical potentials by using both real-fluid methods. However, the impact of real-fluid chemical potential by using the RK method is insignificant in comparison with the 3rd-order Virial method. We speculate that the RK method reveals less effectiveness on the simulations in H_2O dilutions at low temperatures without considering the polarity of H_2O and its interactions with

non-polar molecules.

In Fig. 4(d), total effects of real-fluid were considered. The real-fluid oxidation increases by using the 3rd-order Virial method while decreases using the RK method. The simulations at different temperatures and pressures for different fuels in N_2/CO_2 diluent gases are also performed (see Figs. 5, 6, and S1 in the supporting material), where the reactivities all increase using both the 3rd-order Virial and the RK methods. As such, the RK method exhibits contradictory speciation and ignition simulation predictions in H_2O and N_2/CO_2 diluent gases, respectively, while the 3rd-order Virial method keeps its consistency. Unfortunately, no experimental data on the ignition delay times is available to validate the real-fluid effects on the fuel oxidation simulations in H_2O diluent gas at high pressures. We suspect the contradictory prediction by using the RK method is due to the large uncertainty in describing the real-fluid chemical potentials in the RK method, as is shown in Fig. 4(c). Lack of consideration of molecular polarity of H_2O and its interactions with non-polar molecules may be the main reason for the failure of the RK method on the simulations in H_2O dilute gas at low temperatures. Experimental data in H_2O diluent gas at high pressures (above 100 atm) are necessary to further verify this conjecture.

The simulations of the ignition delay times for the methane oxidation and their comparison with experimental data [35] in CO_2 diluent at 110 and 250 atms are shown in Fig. 5. The ignition delay times are defined based on the maximum of the change of pressures. HP mechanism [36] is used in the simulations. The potential parameters required in the 3rd-order Virial method are extracted from the transport file [37] of the HP mechanism. The ignition delay times are shortened by including the real-fluid behavior by using both real-fluid methods at both pressures in the simulations. At 110 atm, the simulations by employing both real-fluid methods show better performance in predicting the ignition delay times than by using the ideal gas method, while at 250 atm, both real-fluid methods show more obvious improvement as the non-ideal behavior becomes more severe at higher pressures. This figure indicates good consistency of the RK and the 3rd-order Virial methods in carbon dioxide diluent.

The raptor engine of SpaceX Starship was operated in a CH_4/O_2 mixture above 300 atm. Its ignition characteristics have also been investigated by using the 3rd-order Virial method in the present work. As is shown in Fig. 6, the simulations of CH_4/O_2 ignition delay times are performed by using the 3rd-order Virial, RK, and ideal-gas EoSs at 600 atm. The real-fluid ignition delay times increase using both the 3rd-order Virial and the RK methods. Especially, the ignition delay time is decreased by a factor of 3 at 800 K by using the 3rd-order Virial method than in the ideal-gas case. It indicates the crucial impact of real-fluid behaviors in the design and operation of high-pressure rocket engines.

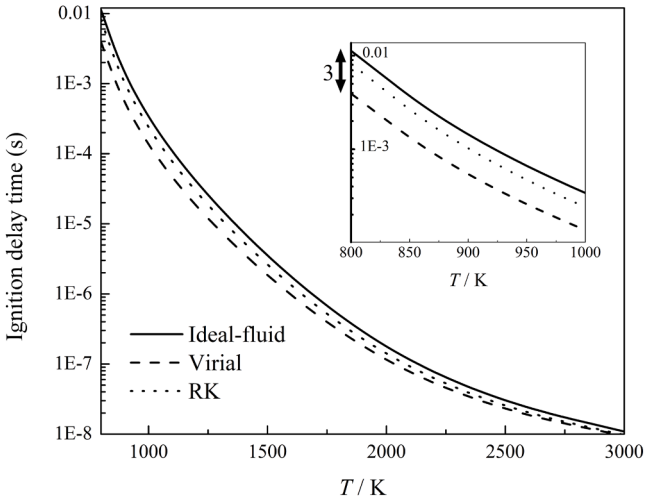

Fig. 6. The simulations of the ignition delay times of the CH_4/O_2 mixture in a 0-D adiabatic, homogenous reactor at 600 atm. CH_4:O_2=1:1.

3.4. The simulations for larger hydrocarbons

The experimental data at high pressures (above 100 atm) for the real-fluid fuel oxidation validations is very rare, resulting in limited comparisons between high-pressure experiments and the simulations of fuel oxidations. To exhaustively characterize canonical spray ignition and combustion experiments at realistic compression-ignition engine conditions, an experiment of the Sandia Spray A [38] was performed, where the baseline condition is n-dodecane injection into an ambient gas at a temperature of 900 K and a pressure of 60 atm. The simulations of the ignition delay times for the n-dodecane oxidation in air at 60 atm and their comparison with experimental data [9] are shown in Fig. 7. A reduced n-dodecane-PAH mechanism [39] is used in the 3rd-order Virial method simulations, which is consistent with the mechanism used by Kogekar et al. [9] in the simulations employing the RK method. Negative temperature coefficient (NTC) effects are shown in both theoretical and experimental results. The simulations using the RK method show better agreements with experimental data at high temperatures (above 1000 K)

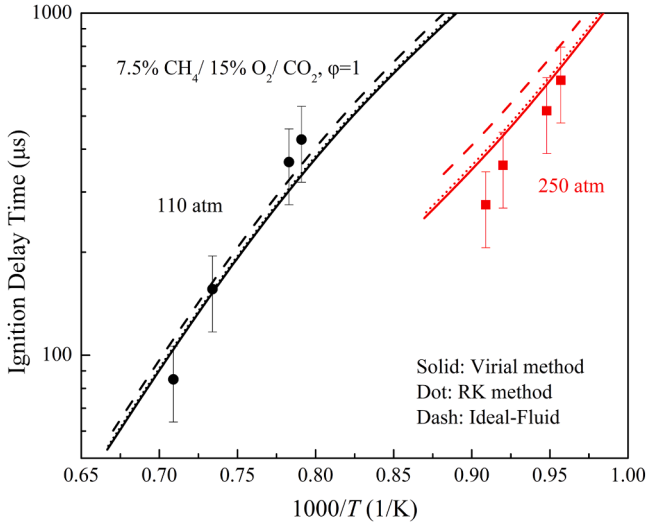

Fig. 5. The comparison of the ignition delay time simulations for the methane oxidation in carbon dioxide diluent with experimental data [35] at high pressures by using RK, 3rd-order Virial, and Ideal-gas methods.

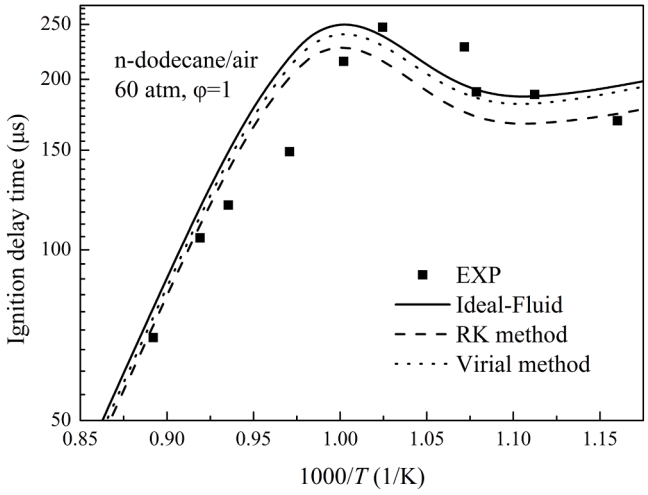

Fig. 7. The comparison of the ignition delay time simulations for the n-dodecane oxidation with experimental data [9] by using RK, 3rd-order Virial, and Ideal-gas methods.

while remaining larger deviations at low temperatures. The difference due to the inaccuracy of the chemical kinetics is also significant, comparing with the effects of real-fluid behaviors, **especially** at the relatively low pressures. The same problem exists in our other comparisons with experimental data in Fig. 8. Additionally, the real-fluid ignition delay times increase by using both real-fluid methods. This is consistent with our discussion for Fig. 5 in N_2/CO_2 diluent gases.

The simulations of the ignition delay times for the gasoline/ethanol blend oxidation in Ar/N_2 at 90 to 110 bar and their comparison with RCM experimental data [40] are shown in Fig. 8. A gasoline mechanism [40] with 1956 species and 10,294 reactions has been reduced to 577 species and 3562 reactions to decrease real-fluid computational cost. It could be seen that the results simulated by using the original mechanism and reduced mechanism show good agreement. The ignition delay times are shortened by including the real-fluid behavior by using the 3rd-order Virial method. Compared with the ammonia oxidation simulations, the impact of real-fluid effects is larger in the gasoline/ethanol blend oxidation simulations, due to higher compression pressures and lower compression temperatures.

The simulation results of gasoline/ethanol blend oxidation using H_2O as diluent gas at 300 atm by including real-fluid effects in the 3rd-order Virial methods are compared with ideal-gas results and are shown in Fig. 9. The real-fluid oxidation is inhibited using the 3rd-order Virial method. The ignition delay time is increased by 86 % at 800 K by using the 3rd-order Virial method. This indicates that a significant difference exists due to real-fluid behaviors at high pressures using H_2O as a diluent gas.

3.5. The simulations for ammonia

Ammonia (NH_3) is considered a promising alternative fuel to reduce the carbon footprint of combustion engines, while possesses very distinct real-fluid behavior at high pressures due to its strong non-polarity. Thus, the combustion properties of ammonia at high pressures and supercritical conditions need to be properly characterized [41]. The simulations of the ignition delay times for the ammonia oxidation in Ar at 55 to 75 bar and their comparison with RCM experimental data [42] are shown in Fig. 10. A recent ammonia mechanism [43] is used in the simulations. The reactivities of the system increase by using the 3rd-order Virial method.

The impact of real-fluid in N_2 diluents is relatively small. However, in many supercritical combustion environments, such as supercritical water environments in liquid-fuel rockets and solid propellant combustion, the real-fluid behaviors have a greater influence. The simulation results of ammonia oxidation using H_2O as diluent gas at 300 atm by including real-fluid effects in the 3rd-order Virial methods are compared with ideal-gas results and are shown in Fig. 11. The real-fluid oxidation is inhibited using the 3rd-order Virial method at lower temperatures. The ignition delay time is increased by 26 % at 800 K by using the 3rd-order Virial method. The major impact comes from the increase of heat capacity in H_2O diluent gas.

The comparisons of the ignition delay time simulations for methanol,

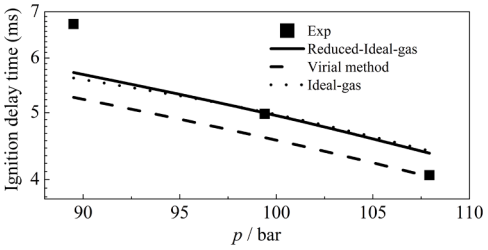

Fig. 8. The comparison of the ignition delay time simulations for the gasoline/ethanol blend oxidation with experimental data [40] by using the 3rd-order Virial and ideal-gas methods. Tc=800 K.

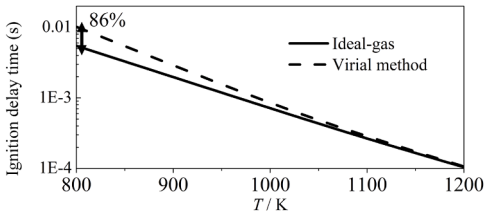

Fig. 9. The simulations of the ignition delay times of gasoline/ethanol blend in a 0-D adiabatic, homogenous reactor using H_2O as diluent gas at 300 atm by using the 3rd-order Virial and ideal-gas EoSs.

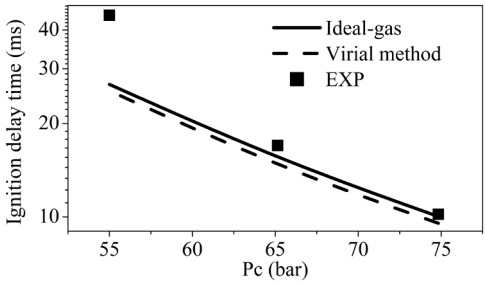

Fig. 10. The comparison of the ignition delay time simulations for the ammonia oxidation with experimental data [42] by using the 3rd-order Virial and Ideal-gas methods. NH_3:O_2:Ar = 0.16:0.04:0.8. Tc=1200 K.

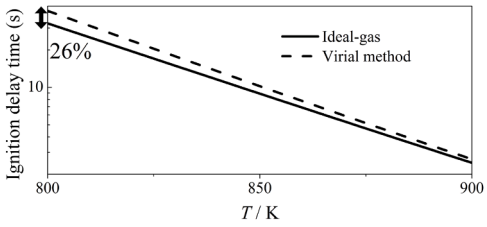

Fig. 11. The simulations of the ignition delay times of ammonia in a 0-D adiabatic, homogenous reactor using H_2O as diluent gas at 300 atm by using the 3rd-order Virial and ideal-gas EoSs.

DME, propane/ethane/methane, propane, and n-butane oxidation with experimental data are shown in the supporting material. The 3rd-order Virial method provides better predictions for the oxidation of C_1 to C_4 fuels and n-dodecane in most cases. However, the real-fluid effects shown in some cases are relatively small. This is mainly caused by their low-pressure experimental conditions and hence relatively small real-fluid deviations of mixtures from ideal gas. The real-fluid behavior is more distinct at higher pressures and lower temperatures where fluid properties are closer to liquid. However, ignition delay time measurements of fuels above 100 atm are quite lacking in literature. A series of flow reactor experimental data against induction time in supercritical water is available in the literature [44-46]. However, the onset of the reaction timing in the flow reactor inlet is very difficult to fix in an experiment. Therefore, the simulation curves must shift to correspond with the experimental curve against the induction time. Such uncertainties directly erase the impact of real-fluid behavior on the deviation of the ideal-gas curves [47]. Therefore, more experiments for the oxidation of different fuels above 100 atm are necessary to further validate the 3rd-order Virial method.

The 3rd-order virial real-fluid method in the 0-D simulations has been completely realized in this work. However, the research on real-fluid effects on transport properties and the 1-D simulations is still unrealized. Developing complete methods and codes based on the Cantera program to describe real-fluid effects on compressibility factors, thermodynamics properties, chemical potentials, and transport properties,

and further studying real-fluid effects on the 1-D simulations, and comparing with experimental data in 1-D system will be our future work.

In addition, the existing Virial method is constructed under the Boltzmann distribution by employing the l-J potential. Unfortunately, at higher pressures (above 300 atm), the Boltzmann assumption for diluted gases does not hold and the l-J potential is not accurate enough to describe intermolecular interactions. Therefore, the existing Virial method does not show advantages above 300 atm. By including the non-Boltzmann distribution in the real-fluid partition function calculation and more accurate intermolecular potential models, the Virial method can be utilized at much higher pressures, while traditional empirical methods may only be effective close to critical points within the training datasets. The development of the non-Boltzmann Virial method is also our future work.

4. Conclusion

The 3rd-order Virial equation of state with nonlinear effects is constructed and applied to the Cantera program for describing supercritical oxidation behaviors in this work. The compressibility factors calculated using the 3rd-order Virial EoS possess better agreements with experimental data for H_2, N_2, and H_2O at different temperatures within 300 atm than the RK EoS and the previous 2nd-order Virial EoS. The calculations of thermodynamic properties by using the 3rd-order Virial EoS also showed a better agreement with experimental data for H_2O than using the RK EoS.

The real-fluid effects on compressibility factors, thermodynamic properties, and chemical potentials for methane oxidation have been respectively discussed by using the RK and 3rd-order Virial methods. The RK method exhibited contradictory speciation predictions against the ideal-gas 0-D and 1-D simulations in H_2O and N_2/CO_2 diluent gases, respectively, while the 3rd-order Virial method kept its consistency as the former lacks the consideration of the molecular polarity of H_2O and its interactions with non-polar molecules.

The comparisons between the real-fluid simulations of alkanes, ammonia, and larger gasoline blends and their experimental data in literature have also been provided. Both real-fluid methods show obvious improvement in the methane oxidation in CO_2 diluent at 250 atm. Especially, the ignition delay simulation by using the 3rd-order Virial EoS is extended to the operation conditions relevant to the recent SpaceX Starship Raptor engines in CH_4/O_2 mixture at 600 atm. It shows the decrease in the ignition delay times by 3 times by including the real-fluid impact. Therefore, it indicates the importance of real-fluid considerations in the designs and operations of high-pressure rocket engines by using high-accuracy computational methods.

The simulation results of gasoline/ethanol blend oxidation using H_2O as diluent gas at 300 atm indicate that a significant difference may be caused by real-fluid behaviors at high pressures using H_2O as diluent gas. The real-fluid oxidation is inhibited using the 3rd-order Virial method for gasoline/ethanol blend oxidation in H_2O diluents at 300 atm. The ignition delay time is increased by 86 % at 800 K by using the 3rd-order Virial method.

Overall, the 3rd-order Virial method is constructed with deeper-level physical insights compared with empirical methods. Instead of inputting critical property parameters manually from literature or computational estimations with high inconvenience and uncertainties in the typical empirical methods, the required potential parameters of different species in the 3rd-order Virial method can be directly and conveniently obtained from the input transport document.

CRediT authorship contribution statement

Junfeng Bai: Writing – original draft, Software, Methodology, Investigation. **Xin Zhang:** Software. **Chong-Wen Zhou:** Methodology, Investigation. **Peng Zhang:** Writing – review & editing, Methodology, Investigation. **Hao Zhao:** Writing – review & editing, Supervision, Methodology, Investigation.

Declaration of interest statement

The authors declare that they have no known competing financial interests or personal relationships that could have appeared to influence the work reported in this paper.

Acknowledgments

This work was supported by the National Natural Science Foundation of China (no. 22350710788), the Fund of Ministry of Education (no. 8091B032244), the Open Fund of the State Key Laboratory of Engines of China (no. K2023-11), the Open Fund of the Ministry Key Laboratory of Marine Power Engineering and Transport Technology (no. KLMPET2022-01), and the Space Power Fund of the China Space Foundation (no. KDJJ20230202005).

Supplementary materials

Supplementary material associated with this article can be found, in the online version, at doi:10.1016/j.combustflame.2024.113728.

References

[1] M. Li, H. Wu, T. Zhang, B. Shen, Q. Zhang, Z. Li, A comprehensive review of pilot ignited high pressure direct injection natural gas engines: factors affecting combustion, emissions and performance, Renew. Sust. Energ. Rev. 119 (2020) 109653.
[2] S.M. Correa, A review of NOx formation under gas-turbine combustion conditions, Combust. Sci. Technol. 87 (1993) 329–362.
[3] J.C. Oefelein, V. Yang, Modeling high-pressure mixing and combustion processes in liquid rocket engines, J. Propul. Power 14 (1998) 843–857.
[4] W. Liang, W. Li, C.K. Law, Laminar flame propagation in supercritical hydrogen/air and methane/air mixtures, Proc. Combust. Inst. 37 (2019) 1733–1739.
[5] M.P. Burke, M. Chaos, Y. Ju, F.L. Dryer, S.J. Klippenstein, Comprehensive H_2/O_2 kinetic model for high-pressure combustion, Int. J. Chem. Kinet. 44 (2012) 444–474.
[6] H. Zhao, C. Yan, T. Zhang, G. Ma, M.J. Souza, C.-W. Zhou, Y. Ju, Studies of high-pressure n-butane oxidation with CO_2 dilution up to 100 atm using a supercritical-pressure jet-stirred reactor, Proc. Combust. Inst. 38 (2021) 279–287.
[7] J.L. Heldmann, M.M. Marinova, D.S. Lim, D. Wilson, P. Carrato, K. Kennedy, A. Esbeck, T.A. Colaprete, R.C. Elphic, J. Captain, Mission architecture using the SpaceX starship vehicle to enable a sustained human presence on Mars, New Space 10 (2022) 259–273.
[8] N. Sakoda, K. Shindo, K. Shinzato, M. Kohno, Y. Takata, M. Fujii, Review of the thermodynamic properties of hydrogen based on existing equations of state, Int. J. Thermophys. 31 (2010) 276–296.
[9] G. Kogekar, C. Karakaya, G.J. Liskovich, M.A. Oehlschlaeger, S.C. DeCaluwe, R. J. Kee, Impact of non-ideal behavior on ignition delay and chemical kinetics in high-pressure shock tube reactors, Combust. Flame 189 (2018) 1–11.
[10] R.L. Scott, P.H. van Konynenburg, Static properties of solutions. Van der Waals and related models for hydrocarbon mixtures, Discuss Faraday Soc. 49 (1970) 87–97.
[11] K.S. Pitzer, R. Curl Jr, The volumetric and thermodynamic properties of fluids.: III. Empirical equation for the second virial coefficient, molecular structure and statistical thermodynamics: selected papers of Kenneth S Pitzer, World Scientif. (1993) 311–312.
[12] O. Redlich, J.N. Kwong, On the thermodynamics of solutions. V. An equation of state. Fugacities of gaseous solutions, Chem. Rev. 44 (1949) 233–244.
[13] G. Soave, Equilibrium constants from a modified Redlich-Kwong equation of state, Chem. Eng. Sci. 27 (1972) 1197–1203.
[14] D.-Y. Peng, D.B. Robinson, A new two-constant equation of state, Ind. Eng. Chem. Fundam. 15 (1976) 59–64.
[15] G. Li, Y. Lu, P. Glarborg, Development of a detailed kinetic model for hydrogen oxidation in supercritical H_2O/CO_2 mixtures, Energy Fuel. 34 (2020) 15379–15388.
[16] V. Giovangigli, L. Matuszewski, F. Dupoirieux, Detailed modeling of planar transcritical H_2–O_2–N_2 flames, Combust. Theory Model. 15 (2011) 141–182.
[17] K.G. Joback, A Unified Approach to Physical Property Estimation using Multivariate Statistical Techniques, 1984.
[18] K.G. Joback, R.C. Reid, Estimation of pure-component properties from group-contributions, Chem. Eng. Commun. 57 (1987) 233–243.
[19] J. Rowlinson, The second virial coefficients of polar gases, Trans. Faraday Soc. 45 (1949) 974–984.
[20] R.B. Bird, E.L. Spotz, J. Hirschfelder, The third virial coefficient for non-polar gases, J. Chem. Phys. 18 (1950) 1395–1402.

[21] J.O. Hirschfelder, C.F. Curtiss, R.B. Bird, M.G. Mayer, Molecular Theory of Gases and Liquids, Wiley, New York, 1964.
[22] J. Bai, P. Zhang, C.-W. Zhou, H. Zhao, Theoretical studies of real-fluid oxidation of hydrogen under supercritical conditions by using the virial equation of state, Combust. Flame 243 (2022) 111945.
[23] H. Kallmann, Thermodynamic Properties of Real Gases For Use in High Pressure Problems, National Technical Information Service, 1950.
[24] J.E. Lennard-Jones, On the determination of molecular fields. II. From the equation of state of gas, Proc. Roy. Soc. A 106 (1924) 463–477.
[25] W.H. Stockmayer, Second virial coefficients of polar gases, J. Chem. Phys. 9 (1941) 398–402.
[26] D.G. Goodwin, R.L. Speth, H.K. Moffat, B.W. Weber, Cantera: an object-oriented software toolkit for chemical kinetics, Thermodyn. Transport Process. (2018). https://www.cantera.org.
[27] M. Chase, C. Davies, J. Downey, D. Frurip, R. McDonald, A. Syverud, NIST JANAF Thermochemical Tables ver. 1.0, US Dept. of Commerce, 1985.
[28] E.P. Bartlett, H. Cupples, T. Tremearne, The compressibility isotherms of hydrogen, nitrogen and a 3: 1 mixture of these gases at temperatures between 0 and 400 and at pressures to 1000 atmospheres, J. Am. Chem. Soc. 50 (1928) 1275–1288.
[29] H. Reamer, R. Olds, B. Sage, W. Lacey, Phase equilibrium in hydrocarbon systems. methane–carbon dioxide system in the gaseous region, Ind. Eng. Chem. 36 (1944) 88–90.
[30] W. Kirillin, L. Rumjanzev, Experimental determination of the specific volume of steam from 92 to 524 atmospheres and from 430 to 600 C, Elektricheskie Stantsii 21 (1950) 8.
[31] A. Michels, H. Schamp, W. De Graaff, Compressibility isotherms of oxygen at 0°, 25° and 50 °C and at pressures up to 135 atmospheres, Physica 20 (1954) 1209–1214.
[32] F.G. Keyes, The pressure-volume-temperature values for ammonia to one thousand atmospheres from 30 to 200, J. Am. Chem. Soc. 53 (1931) 965–967.
[33] B. Golding, B. Sage, Volumetric behavior of nitric oxide, Ind. Eng. Chem. 43 (1951) 160–161.
[34] A. Burcat, Thermochemical Data For Combustion calculations, Combustion Chemistry, Springer, 1984, pp. 455–473.
[35] J. Shao, R. Choudhary, D.F. Davidson, R.K. Hanson, S. Barak, S. Vasu, Ignition delay times of methane and hydrogen highly diluted in carbon dioxide at high pressures up to 300 atm, Proc. Combust. Inst. 37 (2019) 4555–4562.
[36] H. Zhao, J. Fu, F.M. Haas, Y. Ju, Effect of prompt dissociation of formyl radical on 1, 3, 5-trioxane and CH_2O laminar flame speeds with CO_2 dilution at elevated pressure, Combust. Flame 183 (2017) 253–260.
[37] R.A. Svehla, Estimated Viscosities and Thermal Conductivities of Gases At High Temperatures, National Aeronautics and Space Administration, 1963.
[38] L. Pickett, Engine Combustion Network Data Archive, 2016. http://www.sandia.gov/ecn/index.php.
[39] H. Wang, Y. Ra, M. Jia, R.D. Reitz, Development of a reduced n-dodecane-PAH mechanism and its application for n-dodecane soot predictions, Fuel 136 (2014) 25–36.
[40] S. Cheng, C. Saggese, D. Kang, S.S. Goldsborough, S.W. Wagnon, G. Kukkadapu, K. Zhang, M. Mehl, W.J. Pitz, Autoignition and preliminary heat release of gasoline surrogates and their blends with ethanol at engine-relevant conditions: experiments and comprehensive kinetic modeling, Combust. Flame 228 (2021) 57–77.
[41] C.W. Gross, S.-C. Kong, Performance characteristics of a compression-ignition engine using direct-injection ammonia–DME mixtures, Fuel 103 (2013) 1069–1079.
[42] L. Dai, S. Gersen, P. Glarborg, H. Levinsky, A. Mokhov, Experimental and numerical analysis of the autoignition behavior of NH3 and NH3/H2 mixtures at high pressure, Combust. Flame 215 (2020) 134–144.
[43] P. Glarborg, J.A. Miller, B. Ruscic, S.J. Klippenstein, Modeling nitrogen chemistry in combustion, Progr. Energy Combust. Sci. 67 (2018) 31–68.
[44] P.A. Webley, J.W. Tester, Fundamental kinetics of methane oxidation in supercritical water, Energy Fuel. 5 (1991) 411–419.
[45] J.W. Tester, P.A. Webley, H.R. Holgate, Revised global kinetic measurements of methanol oxidation in supercritical water, Ind. Eng. Chem. Res. 32 (1993) 236–239.
[46] H.R. Holgate, J.W. Tester, Oxidation of hydrogen and carbon monoxide in sub-and supercritical water: reaction kinetics, pathways, and water-density effects. 1. Experimental results, J. Phys. Chem. 98 (1994) 800–809.
[47] P.E. Savage, J. Yu, N. Stylski, E.E. Brock, Kinetics and mechanism of methane oxidation in supercritical water, J. Supercrit. Fluids 12 (1998) 141–153.